A Model-Independent, Multi-Image Approach to MR Inhomogeneity Correction

P. A. Bromiley*and N.A. Thacker

Imaging Science and Biomedical Engineering, Stopford Building,
University of Manchester, Oxford Road, Manchester, M13 9PT.

Abstract. We present a technique for model-independent estimation of the inhomogeneity effect across multiple different acquisitions of the same subject, on the assumption of equal inhomogeneities in each image. The technique operates by integration of smoothed estimates of the local derivative of the bias field. Combination of evidence from multiple images is achieved at the derivative estimation stage via statistical weighting. Quantitative analyses of the approach on simulated data, and qualitative analyses on genuine MR images of the foot and hip, demonstrate the superiority of the combined image approach over the equivalent algorithm applied to individual images. The technique has the potential for application to situations where a bias field correction is needed, but likely to be unstably constructed for the acquisition of interest.

1 Introduction

Magnetic resonance images typically exhibit artefacts in the form of non-anatomic spatial intensity variations, known as the inhomogeneity effect, bias field, or gain field. Several sources contribute to this artefact, including B_0 (static) field inhomogeneity introduced both by the main magnet itself and by susceptibility effects at tissue boundaries, and B_1 (radio-frequency, RF) field inhomogeneity in the receiver coil [1]. Many computer-aided image analysis techniques developed for MR, such as intensity-based segmentation techniques, assume that each tissue can be characterised by a well-defined mean intensity. Therefore, the correction of significant inhomogeneity artefacts in the images under analysis is an important pre-processing step in the application of such techniques. The magnitude of the inhomogeneity effect is dependent on a variety of parameters, including both the physical properties of the object being imaged and the scanning parameters, including echo time and repetition time [1]. This makes accurate modelling of the effect for arbitrary objects extremely problematic, and has led to the development of post-hoc correction algorithms. A wide variety of algorithms have been developed for this task ([2] and references therein). One significant problem for such algorithms is that their ability to measure the inhomogeneity is dependent on the signal-to-noise ratio in the image. Thus, the correction is more difficult in regions of the image containing low average intensities, with the bias field being estimated here via a process that is effectively a smooth interpolation. In order to increase the statistical power of the data available to estimate the inhomogeneity effect, several researchers have investigated methods utilising multiple images e.g. [3,4], on the assumption of equivalent anatomy across the images. However, in some circumstances it may be possible to acquire multiple images with approximately equivalent inhomogeneity fields. For example, in surface coil images (and to a lesser extent birdcage coils used in brain imaging) the main source of inhomogeneity is the RF field inhomogeneity of the receiver coil itself. Therefore, through alteration of the imaging parameters (echo time and inversion time) it is possible to acquire multiple images of the same object with differing intensities for each tissue, but with substantially equivalent inhomogeneity effects. This provides a novel method for dealing with the problems of estimating the inhomogeneity effect in tissues of low average intensity and thus low SNR: a companion image with high intensities in those regions can also be acquired, and the inhomogeneity estimated from the image pair.

In previous work we have presented a model-independent algorithm (i.e. not based upon a particular assumption of the tissues present and their expected distributions), for the estimation of inhomogeneity effects in single images. The issue of model-independence is an important one, since techniques which assume particular distributions may bias the later interpretation of pathological tissue. Our technique is based on the assumption that an image is composed predominantly of regions of homogenous tissue, separated by distinct step boundaries. The algorithm therefore estimates a (statistically weighted) local relative image derivative, taking care to first eliminate boundaries, and integrates this data to generate the bias field. In this paper, we demonstrate that the approach can be extended to simultaneously estimate the inhomogeneity effects present in multiple images of the same subject, on the assumption that they are approximately equivalent. The technique is applied to simulated chequerboard images, and simulated MR brain images acquired from Brainweb [5], and the superiority of the multiple-image approach over the application of the equivalent algorithm to individual images is demonstrated. Qualitative results from genuine MR images of the foot and hip are also presented. We conclude with some observations on the potential applicability of the proposed approach.

---

*E-mail: paul.bromiley@man.ac.uk

2 Method

We assume an image formation process in which a mean regional tissue grey level g_t is corrupted by a smoothly varying multiplicative gain $G(x, y)$ and additive noise $n(x, y)$, where x and y are the image plane coordinates

$$I(x, y) = g_t G(x, y) + n(x, y). \tag{1}$$

If the multiplicative distortion can be reliably calculated in well-measured regions, it is a relatively straightforward task to interpolate the observed trends across the entire image. The first step in the algorithm involves estimation of the image noise σ_I from the width of zero-crossings in horizontal and vertical gradient histograms, followed by application of a 3x3 median filter to remove outlier noise. A $(-1, 1)$ template is then used to estimate the intensity shift across adjacent voxels $\Delta_k(x, y)$ where $k = x$ or y, and normalised to remove tissue dependency, g_t, within homogeneous regions e.g. in the x direction we define

$$\Delta_x^{rel}(x, y) = \frac{\partial G(x, y)/\partial x}{G(x, y)} = \frac{2\Delta_x(x, y)}{I(x, y) + I(x - 1, y)} = \frac{2(I(x, y) - I(x - 1, y))}{I(x, y) + I(x - 1, y)}.$$

Error map images for the above calculations are produced using standard error propagation e.g.

$$\sigma_x^{-2}(x, y) = \frac{(I(x, y) + I(x - 1, y))^4}{16\sigma_I^2 (I(x, y)^2 + I(x - 1, y)^2)} \tag{2}$$

A conservative approach to tissue boundaries and regions of low statistical accuracy is taken: the inverse error is set to 0 for voxels of low signal $I(x, y) < \sigma_I$, or those with edges $> 3\frac{\sigma_I}{\sqrt{2}}$. The Δ_k^{rel} images are passed through a smoothing filter S in order to remove the effects of image structure and thus obtain the low spatial frequency variation i.e. the multiplicative gain map. A smoothing kernel of 5% of the image size is a good rule of thumb across the images studied. The appropriately weighted mean estimate of smooth local relative gradient is given by

$$\Delta_x^S(x, y) = \frac{S \otimes \Delta_x^{rel} \sigma_x^{-2}(x, y)}{S \otimes \sigma_x^{-2}(x, y)}. \tag{3}$$

where $\otimes$ represents a 2D convolution. The weighting reduces the significance of poorly measured gradients during convolution, after which they are removed by division. For an image with uniform intensity in homogeneous tissue, equation 3 is zero for all voxels in a slice. This can be used as the basis for a regularisation term to provide increased mathematical stability. Δ_x^S becomes

$$\Delta_x^S(x, y) \Rightarrow \frac{S \otimes (\Delta_x^{rel} \sigma_x^{-2}(x, y) + 0_{reg})}{S \otimes (\sigma_x^{-2}(x, y) + \sigma_{reg}^{-2})}. \tag{4}$$

The factor σ_{reg} is calculated at $|I(x, y) - I(x - 1, y)| = 3\sigma_I$. This upper limit on the error constrains the effect of any voxels with large errors in their gradient calculations. However, the bias introduced towards zero gradient in regions dominated by noise necessitates a limited number of iterations of the gain correction process in order to converge on the correct value of local gain variation.

At this stage, since error maps for the relative gradient maps are available, the gradient maps from any number of images with approximately equivalent inhomogeneity effects can be combined in a simple weighted averaging process, and the error map for the combined data calculated. A 2D map of the inhomogeneities can then be obtained by re-integrating the x and y gradient maps, using the centre of the image (which is within the region of interest for most MR images) to provide a relative point of unity gain. In order to prevent "integral wind-up" of errors, redundant information available from both directions of re-integration is utilised as described in [6]. The inverse of the exponential of the resulting inhomogeneity map provides the multiplicative correction.

Evaluation of the algorithm comprised two quantitative and two qualitative stages. First, two chequerboard images with opposite intensities were prepared (Fig. 1) and a 40% multiplicative bias field consisting of a pair of Gaussians was applied, followed by the addition of 1% random Gaussian noise. The inhomogeneity correction algorithm was applied to each image individually, and also to the images as a pair. Coefficients of variation (i.e. the ratio of the intensity standard deviation to the mean) were calculated for the light squares in each image, and used to calculate the percentage of the original inhomogeneity remaining after correction. An equivalent experiment was then performed using simulated T1 and T2 brain MR images from Brainweb [5]. Slice 160 of Brainweb inhomogeneity field A was applied multiplicatively to slice 27 from each volume, followed by the addition of 3% Gaussian random noise, and the
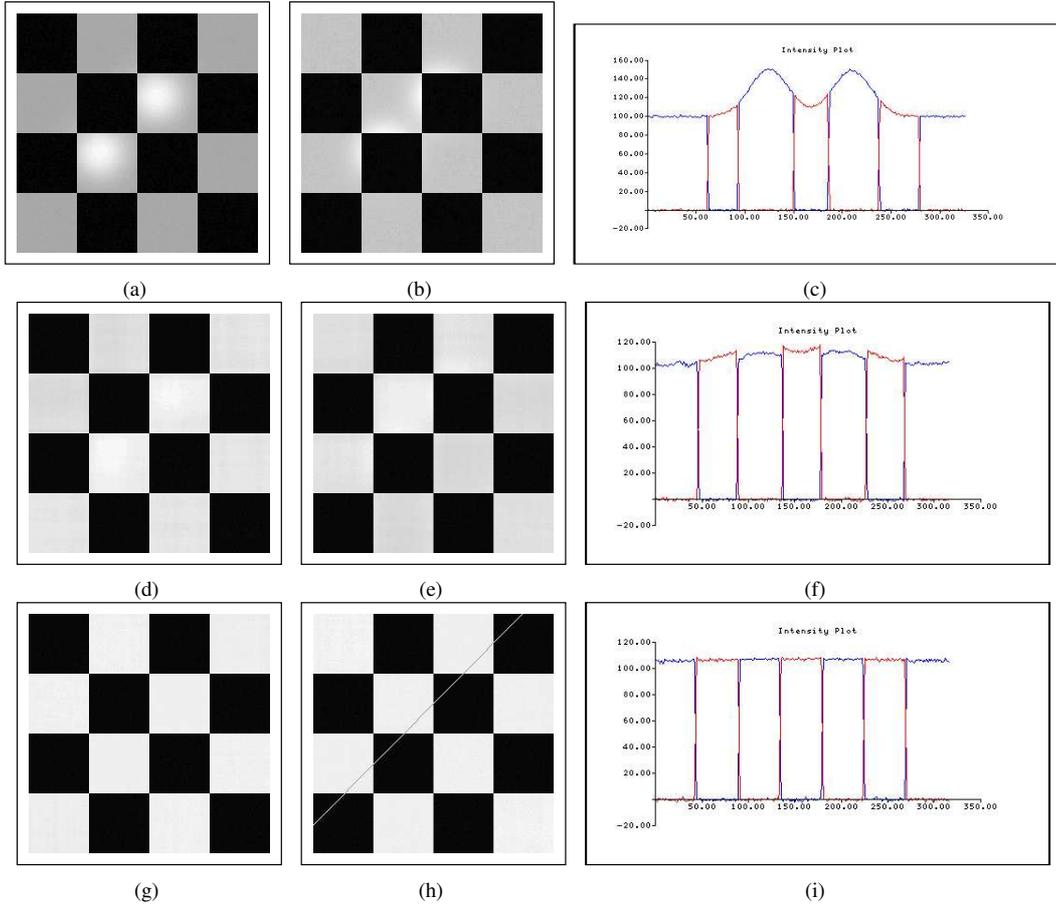
Figure 1. The original chequerboard images (a,b), individually corrected images (d,e), jointly corrected images (g,h) and intensity profiles (c, f, i) for each pair along the line shown in h.

same evaluation procedure used with the chequerboard images was followed, using the Brainweb tissue phantom to identify white matter (WM) and grey matter (GM) in the corrected images. Finally, the algorithm was applied to T1 and T2 MR image pairs of the foot and hip, in order to demonstrate qualitatively the operation of the algorithm on real MR data.

Correction Method	T1 WM	T1 GM	T2 WM	T2 GM
Individual	47.5	89.0	17.0	28.8
Joint	0.5	8.3	0̄	2.5

Table 1: Inhomogeneity (as percentage, $\pm \approx 5\%$) remaining in the WM and GM after correction in the simulated Brainweb images.

3   Results

Figure 1 shows the result of individual and joint inhomogeneity correction of the simulated chequerboard images. As can be seen from the intensity variation along the profiles, the individual corrections fail to remove all of the inhomogeneity: 31% of the inhomogeneity originally present in Figure 1a and 74% of that in Figure 1b remain after correction: the performance is worse on the second image as the peaks of the bias field lie predominantly within the dark squares were the SNR, and so the inhomogeneity after multiplication, is zero. However, when corrected as a pair the inhomogeneity is completely removed to within the noise level. Equivalent results were obtained with the Brainweb images (Fig. 2, Table 1). The SNR is lower in the GM of the T1 image and the WM of the T2 image, and correction of the GM is particularly problematic due since it occupies a relatively thin band in the image. Therefore, whilst the original algorithm corrects the majority of the inhomogeneity in most regions, it removes only 10% of the inhomogeneity in the GM of the T1 image. In contrast, the combined correction removes all the inhomogeneity to within errors due to the higher statistical power available in the combined data set. Finally, Fig. 3 and Fig. 4 show applications of the inhomogeneity correction individually and jointly to T1 and T2 pairs of hip and foot images. These data are presented only for qualitative evaluation: however, in both cases the joint correction is visibly more stable.
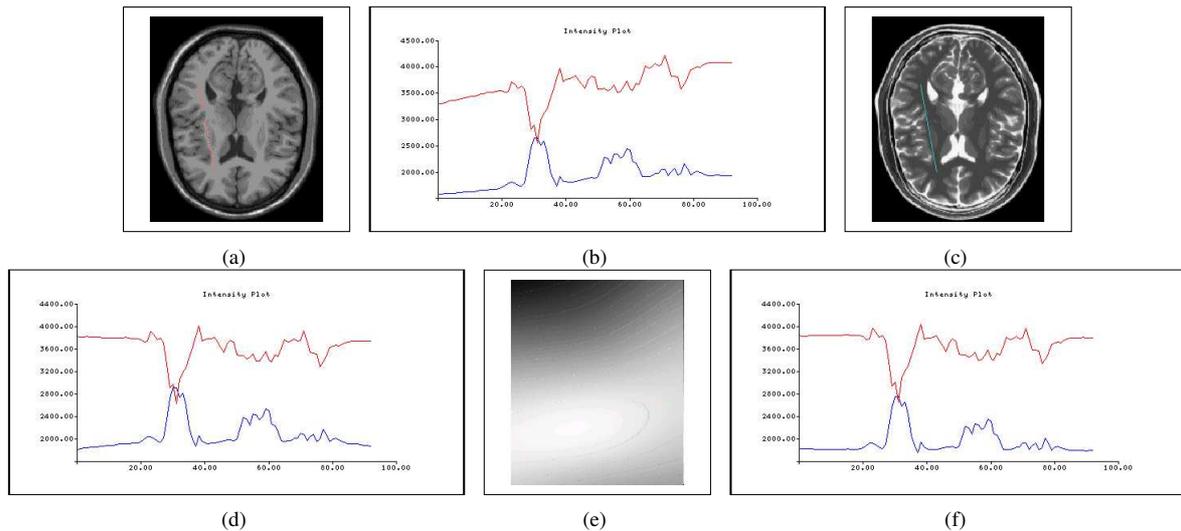
Figure 2. The T1 (a) and T2 (c) Brainweb images, the multiplicative bias field (e), and the profiles along the line shown in (c) for the uncorrected (b), individually corrected (d) and jointly corrected (f) images.

4 Conclusion

In previous work [6] we presented a model-free inhomogeneity correction algorithm. Like other model-free techniques, its successful application is dependent upon having good quality data. In many real world situations this may prove a real impediment to use of the technique. In this paper, we have demonstrated that the algorithm can be extended to simultaneous correction of multiple images on the assumption that the inhomogeneity effects are equivalent across the images. This assumption is approximately valid under certain circumstances, for example when scanning is performed using a surface coil, where the inhomogeneity artefact is dominated by the RF inhomogeneity of the coil itself and so is independent of the scanning parameters to a large extent. Under such circumstance multiple images of the same subject can be acquired with varying intensities in each tissue through variation of the scanning parameters, without greatly affecting the inhomogeneity, ensuring that across the set of images as a whole high SNR is present in all tissues. This increases the statistical power of the data to determine the inhomogeneity effect, and thus results in superior inhomogeneity correction. The resultant increase in performance has been demonstrated quantitatively on simulated data and qualitatively on real MR image pairs of the hip and foot. We anticipate that this approach may also be applicable in some modern MR scanning protocols (e.g. [7]) where multi-contrast images are acquired simultaneously with some sharing of K-space, and so some sharing of inhomogeneity effects between the images.

Acknowledgements

References

1. A. Simmons, P. S. Tofts, G. J. Barker et al. "Sources of intensity nonuniformity in spin echo images at 1.5T." *Magnetic Resonance Imaging* **32**, pp. 121–128, 1994.
2. Z. Hou. "A review on MR image intensity inhomogeneity correction." *International Journal of Biomedical Imaging* **2006**, pp. 1–11, 2006.
3. E. G. Learned-Miller & P. Ahammad. "Joint MRI bias removal using entropy minimisation across images." *Neural Information Processing Systems* **17**, pp. 761–768, 2005.
4. S.-H. Lai & M. Fang. "A dual image approach for bias field correction in magnetic resonance imaging." *Magnetic Resonance Imaging* **21**, pp. 121–125, 2003.
5. C. A. Cocosco, V. Kollokian, R. K.-S. Kwan et al. "Brainweb: Online interface to a 3D MRI simulated brain database." *NeuroImage* **5(4)**, pp. S425, 1997.
6. E. Vokurka, N. A. Thacker & A. Jackson. "A fast model independent method for automatic correction of intensity non-uniformity in MRI data." *Journal of Magnetic Resonance Imaging* **10**, pp. 550–562, 1999.
7. R. Mekle, A. F. Laine & E. X. Wu. "Combined MR data acquisition of multicontrast images using variable acquisition parameters and k-space data sharing." *Magnetic Resonance Imaging* **21**, pp. 121–125, 2003.
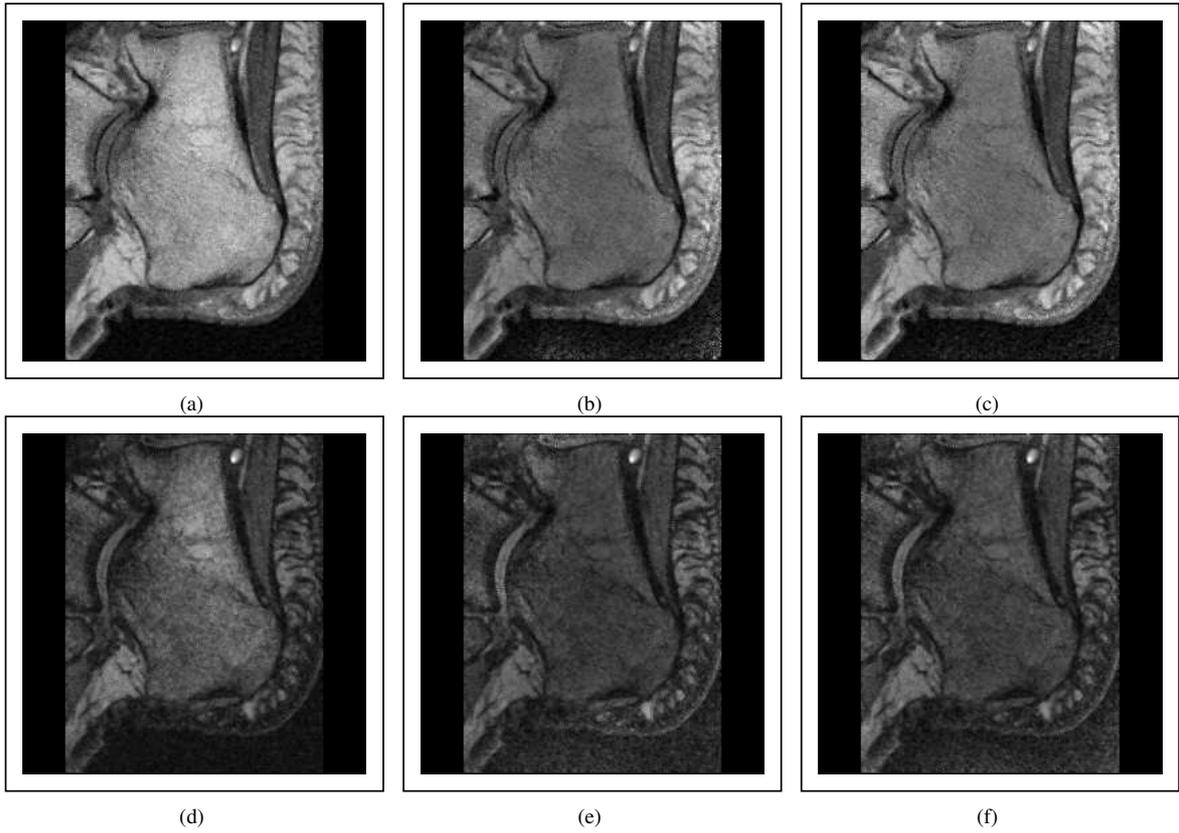
Figure 3. The original (a,d), individually corrected (b,e) and jointly corrected (c,f) MR foot images.
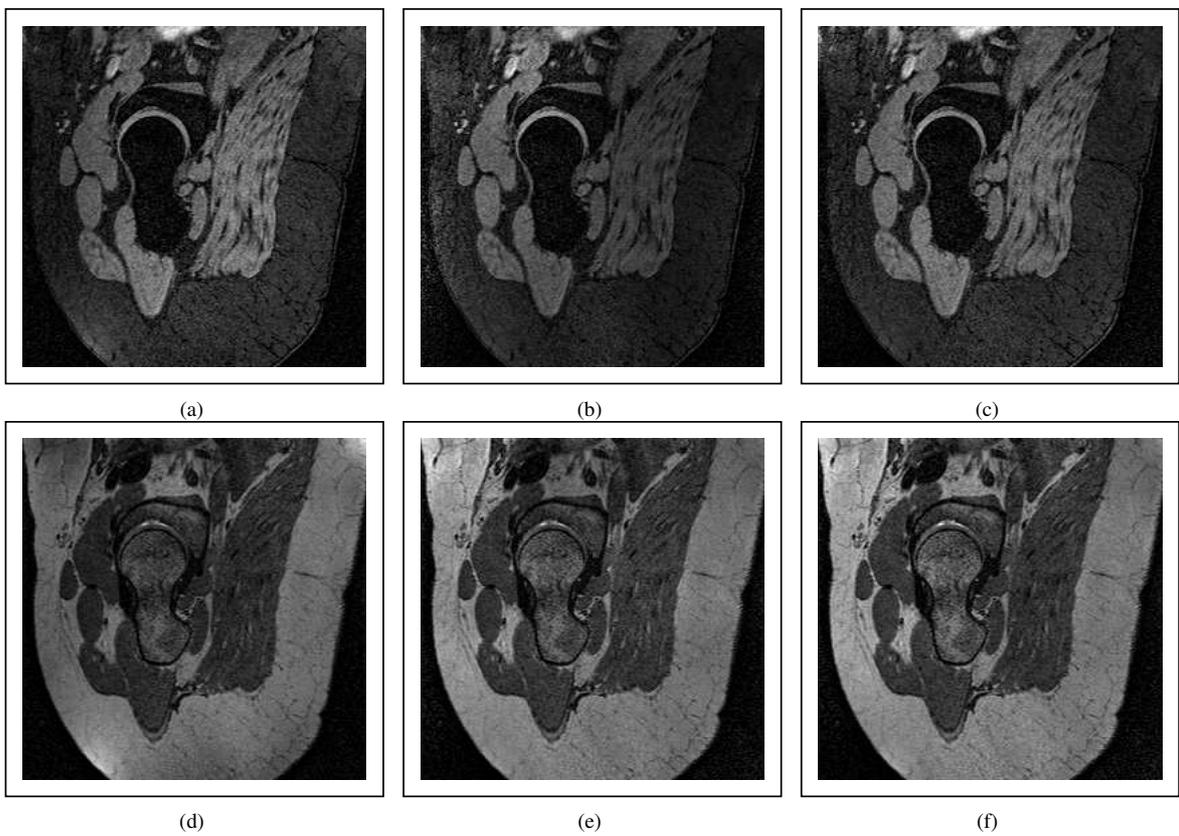

Figure 4. The original (a,d), individually corrected (b,e) and jointly corrected (c,f) MR hip images.